Pergamon

Int. J. Heat Mass Transfer. Vol. 41, Nos 8–9, pp. 993–1001, 1998

Printed in Great Britain
0017-9310/98 $19.00+0.00

PII: S0017-9310(97)00226-3

Evaporation of solution droplets in spray pyrolysis

HSUAN-FU YU* and WEN-HAUR LIAO
Chemical Engineering Department, Tamkang University, Tamsui, Taiwan 25137, R.O.C.

(*Received* 21 *March* 1997 *and in final form* 31 *July* 1997)

Abstract—A mathematical model describing the behavior of evaporating solution droplets in spray pyrolysis was developed and verified. The effects of mass, momentum, and heat transfer, as well as solute precipitation, on evaporating solution droplets were considered simultaneously. The concept of real solution was used in calculations to estimate the saturated vapor pressures of the droplet. The precipitation heat of solute caused the droplet temperature to jump up and enhanced the solvent evaporation rate. While increasing the gas temperature resulted in a steeper concentration gradient inside the droplet, decreasing the concentration of the starting solution reduced the sizes of resultant particles. Accordingly, a two-stage heating arrangement with a dilute starting solution in spray pyrolysis is suggested to produce small solid aerosol-derived particles. © 1997 Elsevier Science Ltd.

1. INTRODUCTION

Spray drying has been widely exploited in the foods, chemicals and materials industries for many years. For instance, instant coffee, coffee whitener, milk powder, soups, baby foods, and sweeteners are produced using this technique. Recent studies and development have shown the potential of using a similar technique, called spray pyrolysis, to produce high quality powder required in advanced ceramic processing, such as ZnO, NiO, Al_2O_3, Fe_2O_3, Fe_3O_4, $NiFe_2O_4$ [1–5]. In spray pyrolysis, the morphology of resultant particles strongly depends on the process precursors and operating conditions. Previous studies by the authors [3–5] and others [2, 6, 7] have shown that the aerosol-derived particles, in many cases, are composed of hollow particles. The hollow particles may be used to prepare low density high temperature insulators, but they hinder the development of mechanical and electrical properties of structural and electronic ceramics. Understanding the thermal history of aerosols in the process and the effects of processing parameters are important to the production of desired ceramic particles. In this study the transport phenomena occurring in and around the aerosol droplets are investigated theoretically and the effects of operating conditions on the resultant particles are studied.

Some efforts have been made to study the evaporation behavior of small liquid droplets. Ranz and Marshall [8] investigated the factors that influence the rates of evaporation of pure liquid droplets and aqueous droplets containing dissolved salts during drying. They have shown that the surface area of a pure droplet decreases linearly with processing time and that the Sherwood number (*Sh*) and the Nusselt number (*Nu*) at zero Reynolds number (*Re*) are equal to 2. Charlesworth and Marshall [9] studied the evaporation of an aqueous droplet. Based on the experimental observations, they proposed a mathematical model to describe the thermal history of a solution droplet, assuming that the mass transfer of solvent and solute inside the droplet was by diffusion only. Since a moving boundary posed mathematical difficulties, they considered the droplet in the model to be of constant diameter and received solutes through the surface at a rate corresponding to the amount of solute in a volume equivalent to that evaporated per unit time. They also summarized how the permeability and thermal characters of metal salts affected particle morphologies.

El Golli *et al.* [10] developed a model to explain the thermal behavior of a saline droplet in spray drying. They used a modified Maxwell diffusion equation to describe the movement of solvent vapor in air. They considered the saline droplet as a bulk material, with no concentration gradient inside the droplet during water evaporation, and they ignored the effects of heat transfer on the behavior of the evaporating droplet. Leong [11] experimented with aqueous droplets and demonstrated that the morphologies of aerosol-derived particles were affected by solute nature, evaporation rate of the solvent, solubility of the solute in the solvent, and mass concentration of the solution used. Messing *et al.* [12, 13] developed a mathematical model to describe the changes of aerosol diameters in spray pyrolysis and used the model to study the effects of various operating parameters. They assumed that mass transfer in the evaporating solution droplet was due to diffusion only and that the solution droplet behaved ideally. On the other hand, Yu [14] formulated mathematically the behavior of aqueous

* Author to whom correspondence should be addressed.

NOMENCLATURE

A	cross-sectional area of wire
C_p^B	heat capacity of solvent B
C_p^C	heat capacity of solvent C
C_p	heat capacity of droplet
D_{BC}	diffusivity of solvent B with respect to solute C
D_{CB}	diffusivity of solute C with respect to solvent B
D_{CB}^0	initial diffusivity of solvent B with respect to solute C
D_v	diffusivity of solvent in gas at T and P
D_v^0	diffusivity of solvent in gas at T^0 and P^0
h_m	heat transfer coefficient for gas to wire
k_a	average thermal conductivity of gas
k_g	mass transfer coefficient
k_m	thermal conductivity of metallic thin wire
L	length of metallic thin wire
M_B	molecular weight of solvent B
m_p	total mass of droplet
P_L	perimeter of metallic thin wire
P^{sat}	saturation vapor pressure of pure solvent
P_g	vapor pressure of solvent in bulk gas
P^0	pressure at reference condition
P_s	saturation vapor pressure of droplet
Q_m	heat transfer rate through metallic thin wire
R	radius of droplet
R_g	gas constant
R.H.	relative humidity
R_0	initial radius of droplet
r	radial distance from center of droplet
t	time
T^g	temperature of bulk gas
T^l	temperature of droplet
T_0^l	initial temperature of droplet
T^0	temperature at reference condition
u	velocity of interface
x_B	molar fraction of solvent B
x_C	molar fraction of solvent C
X_C	solubility of C in water in molar fraction
W_B	mass fraction of solvent B
W_{BO}	initial mass fraction of solvent B
W_C	mass fraction of solute C
W_{CO}	initial mass fraction of solute C
W_B^{av}	average mass of solvent B in droplet
W_C^{ac}	average mass of solute C in droplet.

Greek symbols

γ_B	activity coefficient of solvent B
η	kinematic viscosity of droplet
λ	latent heat of droplet
v_A^g	velcity of gas A
v_C^l	velocity of solute C
v^g	mass average velocity in ambient gas
v^l	mass average velocity in liquid droplet
v_B^l	mass velocity of solvent B in liquid droplet
v_C^l	mass velocity of solute C in liquid droplet
ρ^g	density of ambient gas
ρ^l	density of droplet
ρ_0^l	initial density of droplet
$\tilde{\rho}^l$	average density of droplet.

droplets during solvent evaporation. He assumed that the liquid droplet behaved like an ideal solution and considered the effects of mass momentum, and energy transfer inside and around the droplet. He demonstrated theoretically that the concentration gradient, having the highest solute concentrations on the droplet surface, is developed during evaporation. Later, Yu [15], by simply considering the changes of phases of the droplet, estimated the effects of precipitation and decomposition of the solute on the sizes and size distribution of aerosol-derived particles.

In view of the above, the mathematical models published to describe the behavior of solution droplets during solvent evaporation treated the behavior of solution droplets as an ideal solution. However, the behavior of solution droplets, in most of the cases, departs from that of an ideal solution, especially for those having high solute contents. The main objectives of this work were to consider the effects of real solution behavior and heat of precipitation on the solute distribution of an evaporating solution droplet. The transport paths of species in the droplet were also discussed through the results obtained from our model.

2. MODEL DEVELOPMENT

In spray pyrolysis, the aerosol experiences the evaporation of solvent, the precipitation of solutes, the formation of a solid crust, the decomposition of precipitated solutes, and even, in higher temperatures, the solid-state reactions between the precipitated solids [15]. The evaporation of solvent results in a size reduction of the droplet and the development of a concentration gradient within the droplet, with the highest solute concentration on the droplet surface. When the surface solute concentration exceeds the solubility limit, the solute precipitates, as solid islands, on the surface of the droplet. Continuing solvent evaporation increases the number of precipitated islands

and causes the solid islands to approach and touch each other, resulting in the formation of a porous crust. The remaining solvent then continues to evaporate through the open-connected pores in the crust. As the crust temperature increases, the solid crust may undergo further changes (e.g., decomposition, solid-state reactions, and sintering). Because of the complexity of multiphase transport procedures and the lack of information on the crust structure, the changes of aerosols due to the decomposition and solid-state reactions of precipitated solutes were not considered here. The present work mathematically modeled the changes of solution droplets before the formation of a solid crust.

During modeling, some assumptions and justifications were introduced on account of the lack of data for some parameters involved. They are:

(a) the flow of gas is laminar and there are no interactions between the droplets;
(b) the relative velocity between the aerosol and carrier gas is zero; this is valid when the aerosol droplets in the process are traveling perpendicular to the direction of gravity;
(c) the ambient gas around the droplet obeys the ideal gas law and is under near isobaric conditions;
(d) the temperature of the liquid droplet is only a function of time since the Biot number of the system is much less than 0.1;
(e) all fluids involved are Newtonian fluids;
(f) the heat transfer by radiation is small and can be ignored;
(g) the Kelvin effect (due to the curvature of the droplet surface) on the equilibrium vapor pressure of the droplet is negligible since the size of the droplet is larger than 1 μm; and
(h) the aerosol has a perfect spherical shape and the changes of concentration and velocities of matters inside the liquid droplet are symmetrical.

It is to be noted that the aerosols moving in the process may interact with each other and cause a coalescing of droplets. The interactions between the droplets may be due to the electrostatic effects between them, the Brownian motion of droplets themselves, or the impact of aerosols of different sizes, with different traveling speeds. The coalescence of droplets changes the sizes and size distribution of aerosols and may disturb the concentration field inside the droplets. Depending on the status of aerosol droplets at the moment of coalescence occurring, nodular hollow spherical particles may be produced [4]. The effects of interactions between the droplets were not considered at this stage of study and should be included in future study.

By choosing the center of the droplet as the origin of moving spherical coordinates and applying the above assumptions and justifications, the mass transfer, momentum transfer and heat transfer in and around the droplet were mathematically described, as shown in Table 1.

Since the transfer of solvent is across the interface between the droplet and its ambient gas, the movement of solvent on the interface can be written, using the jump mass balance, as

$$\rho^{l}(-v^{l}+u)+\rho^{g}(v^{g}-u)=0, \tag{1}$$

$$v_{A}^{g}=u, \tag{2}$$

$$v_{C}^{l}=u, \tag{3}$$

where u is the displacement velocity of interface and is equal to

$$u=\frac{dR}{dt}. \tag{4}$$

From eqns (1)–(3) as well as the definition of mass average velocity, it can be shown that

$$v^{l}=u+\frac{k_{g}M_{B}}{R_{g}\rho^{l}}\left(\frac{P_{s}}{T^{l}}-\frac{P_{g}}{T^{g}}\right), \tag{5}$$

which describes the change at the interface and is used as one of the boundary conditions (at $r=R$) for the equation of motion (in the r-direction).

This problem is a non-linear moving boundary problem and poses a difficulty in directly handling the corresponding equations. To take account of this difficulty, the problem was converted to a fixed boundary problem by redefining the process variables, in dimensionless forms, as shown in Table 2. Substituting r^{*} for r in the corresponding equations makes sure that the surface of the solution droplet is always at $r^{*}=1$, regardless of the degree of evaporation. The transport equations, in dimensionless forms, with the corresponding initial and boundary conditions were solved simultaneously, using a finite difference scheme [16, 17]. Iteration method was used in calculation to approach the solutions of the equations.

3. PROPERTIES OF PROCESS FLUIDS

For a real solution droplet, the saturated vapor pressure of the solvent (just above the droplet surface) can be expressed as

$$P_{s}=\gamma_{B}x_{B}P^{sat}. \tag{6}$$

The changes of activity coefficient (γ_{B}) with the temperature and surface concentration of the droplet can be correlated using the van Laar equation,

$$\ln\gamma_{B}=\frac{AB}{\left(A+\dfrac{x_{B}}{x_{C}}\right)^{2}}\frac{1}{T}, \tag{7}$$

where A and B are parameters in the van Laar equation. A and B are 1.2×10^{1} and -1.0×10^{3} for $NH_4NO_{3(aq)}$, and 5.8 and -2.9×10^{3} for $NaCl_{(aq)}$ (obtained by correlating the activity data published in *Handbook of Chemistry and Physics*, 71st edn, CRC, Boston, 1990), respectively.

Table 1. Governing equations and their initial and boundary conditions

Mass transport in the liquid droplet

$$\rho^{l}\left(\frac{\partial W_B}{\partial t}+v^{l}\frac{\partial W_B}{\partial r}\right)=\frac{D_{BC}}{r^2}\frac{\partial}{\partial r}\left(r^2\rho^{l}\frac{\partial W_B}{\partial r}\right)$$

I.C.:

$$\text{at}\quad t=0,\quad W_B=W_{BO}$$

B.C.:

$$\text{at}\quad r=0,\quad \frac{\partial W_B}{\partial r}=0$$

$$\text{at}\quad r=R,\quad [W_B(v_B^{l}-v_C^{l})+v_C^{l}]^{-1}=\frac{k_g M_B}{R_g\left(v^{l}-\dfrac{dR}{dt}\right)}\left(\frac{P_s}{T^{l}}-\frac{P_g}{T^{g}}\right)$$

Momentum transport in the droplet

$$\frac{\partial v^{l}}{\partial t}+v^{l}\frac{\partial v^{l}}{\partial r}=\frac{4}{3}\eta\left(\frac{\partial^2 v^{l}}{\partial r^2}+\frac{2}{r}\frac{\partial v^{l}}{\partial r}-\frac{2v^{l}}{r^2}\right)$$

I.C.:

$$\text{at}\quad t=0,\quad v^{l}=0$$

B.C.:

$$\text{at}\quad r=0,\quad \frac{\partial v^{l}}{\partial r}=0$$

$$\text{at}\quad r=R,\quad v^{l}=\frac{dR}{dt}+\frac{k_g M_B}{R_g\rho^{l}}\left(\frac{P_s}{T^{l}}-\frac{P_g}{T^{g}}\right)$$

Mass transport in the gas phase

$$\frac{dR^2}{dt}=\frac{-2D_v M_B}{R_g\tilde{\rho}^{l}}\left(\frac{P_s}{T^{l}}-\frac{P_g}{T^{g}}\right)$$

I.C.:

$$\text{at}\quad t=0,\quad R=R_0$$

Heat transport in the system

$$(4\pi R)k_d(T^{g}-T^{l})+\lambda\frac{dm_p}{dt}=m_pC_p\frac{dT^{l}}{dt}$$

I.C.:

$$\text{at}\quad t=0,\quad T^{l}=T_0^{l}$$

The effects of temperature and solution concentrations on the other parameters (e.g., C_p, D_v, k_d, etc.) involved in the process were considered using the relationships shown in Table 3. The specific volume of the solution droplet was assumed to be independent of temperature and to be linear to the compositions of the droplet which allows the droplet density to be calculated from the information on the composition of the solution droplet. On the other hand, the kinematic viscosity (η) of the liquid droplet was assumed to be constant for simplicity since the viscosity and density of a solution usually increase with its solute composition.

4. MODEL VERIFICATION

The model developed here was verified by $NH_4NO_{3(aq)}$ and $NaCl_{(aq)}$ droplets, using the experimental data obtained by Ranz and Marshall [8] for droplets suspended in still air. All calculations were performed on a Sun Sparc-20.

4.1. $NH_4NO_{3(aq)}$ *droplet*

Table 4 gives the experimental conditions used by Ranz and Marshall for $NH_4NO_{3(aq)}$ droplets. Figure 1 shows the change of droplet surface area during evaporation, observed by Ranz and Marshall and computed by the model developed here. Curve (a) considered that the mass transfer inside the droplet was through diffusion only and curve (b) considered both diffusion and convection. It is clear that the mass transfer inside the solution droplet is not only by diffusion.

The discrepancy between the experimental data and curve (b) was attributed to the difference in the opera-

Table 2. Dimensionless variables

Variables and parameters	Definition
Radial distance	$r^* = \frac{r}{R}$
Time	$t^* = \frac{tD^0_{CB}}{R_0^2}$
Density	$\rho^* = \frac{\rho^l}{\rho^l_0}$
Velocity	$v^* = \frac{v^l R_0}{D^0_{CB}}$
Droplet temperature	$T^* = \frac{T^l}{T^l_0}$
Gas temperature	$T^*_g = \frac{T^g}{T^l_0}$
Droplet radius	$R^* = \frac{R}{R_0}$

ting conditions: the $NH_4NO_{3(aq)}$ droplet in the experiments of Ranz and Marshall was supported by a metallic thermoelement, but the solution droplet considered in the proposed model was a free droplet suspended in the gas. The metallic wire in the experiments provided an additional path for heat transfer between the droplet and the ambient. To take into account this effect, eqn (8) describing the amount of heat through the wire was added into the energy transfer equation and the calculated results are then presented as curve (c) in Fig. 1. Except near the crust formation, curve (c) well describes the experimental data.

$$Q_m = \sqrt{h_m P_L k_m A}(T^g - T^l)\tanh\left(\sqrt{\frac{h_m P_L L}{k_m A}}\right). \quad (8)$$

Table 4. Ranz and Marshall experimental conditions

For $NH_4NO_{3(aq)}$ droplet	
Temperature of air	293 K
Humidity of air	0%
System pressure	738 mmHg
Initial radius of droplet	0.0563 cm
Initial temperature of droplet	281 K
Total solute in droplet	3×10^{-4} g
For $NaCl_{(aq)}$ droplet	
Temperature of air	293 K
Humidity of air	0%
System pressure	738 mmHg
Initial radius of droplet	0.0574 cm
Initial temperature of droplet	281 K
Total solute in droplet	1.9×10^{-4} g

The small deviation between curve (c) and the experimental data was thought to be due to the heat evolved during the precipitation of solutes. The precipitation heat should enhance the evaporation of solvent and could result in droplet diameter reduction. The model, to consider the effects of precipitation heat, was modified by assuming that the solute begins to precipitate after the surface concentration of the droplet reaches the saturated value at the corresponding droplet temperature, and then estimating the amount of precipitation heat due to the change of heat capacity of the droplet. Figure 2 shows the results after considering the effects of solute precipitation. It is evident that the model proposed now can well depict the dimensional changes of an evaporating solution droplet.

Figure 3 shows the variations of droplet temperature during solvent evaporation. Curve (b), considering the effects of solute precipitation and the heat via the thermoelement, passes through the exper-

Table 3. Relationships between the parameters and operating conditions

Parameters	Relationships	Ref.
Diffusivity of gas	$D_v = D^0_v\left(\frac{T^g}{T^0}\right)^m \frac{P^0}{P_g}$	[18]†
Thermal conductivity	$k_d = 9.8611\times10^{-6}+9.6533\times10^{-6}T^g-3.6275\times10^{-9}T^{g^2}$	‡
Saturation vapor pressure	$P^{sat} = \frac{1}{760}\exp\left[18.3036-\frac{3816.44}{(T^l-46.13)}\right]$	[19]
Heat capacity	$C_p = W^{av}_B C^B_p + W^{av}_C C^C_p$	
Latent heat	$\lambda = 2.9038\times10^4 - 10.315T^l - 2.113\times10^{-2}T^{l^2}$	Steam table‡
Solubility	$\log X_C = a+\frac{b}{T^l}+c\log T^l$ (for $NH_4NO_{3(aq)}$, $a=25.705$, $b=-1650.43$, $c=-8.3494$)	[20]

† $T = \sqrt{T^0 T^l}$.
‡ Curve-fitting the published data by authors.

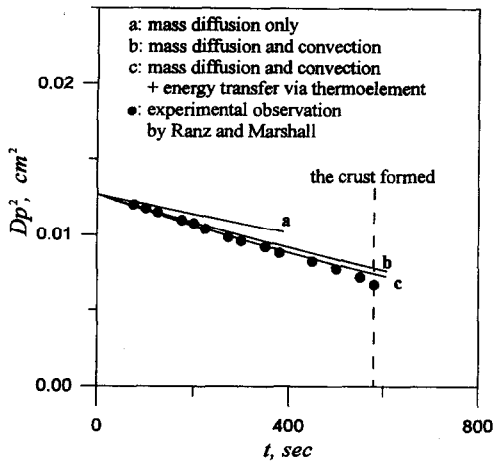

Fig. 1. Experimental and calculated results for $NH_4NO_{3(aq)}$ droplet.

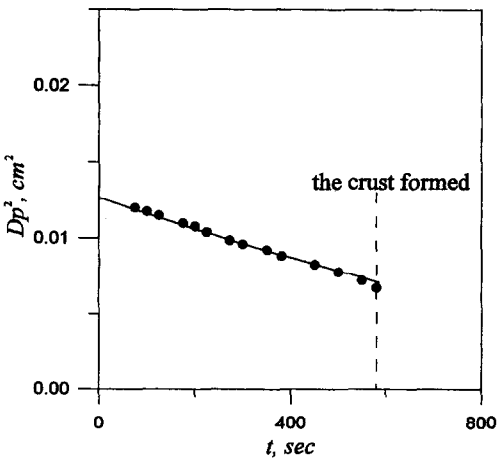

Fig. 2. Data obtained from the experiment and the calculation for $NH_4NO_{3(aq)}$ droplet.

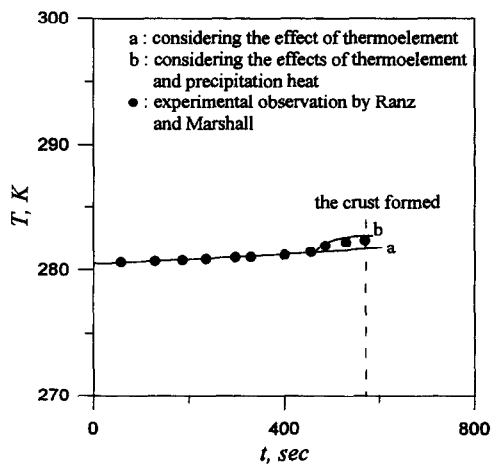

Fig. 3. Changes of droplet temperatures measured from the experiment and calculated from the model presented.

imental data observed by Ranz and Marshall. The results obtained experimentally and theoretically ("●" and "curve b" in Fig. 3) also indicate that while the

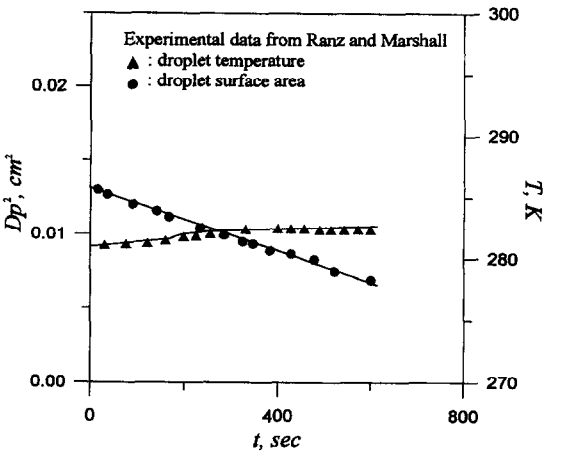

Fig. 4. Experimental and calculated results for $NaCl_{(aq)}$ droplet.

solute starts to precipitate, the droplet temperature jumps up. This sudden increase of droplet temperature, which is due to the precipitation heat, will enhance solvent evaporation.

4.2. $NaCl_{(aq)}$ *droplet*

To further verify the model, it was used to simulate the changes of an evaporating saline droplet and the calculated results were compared with the experimental data obtained by Ranz and Marshall [8]. Table 4 gives the conditions of this saline droplet. Figure 4 shows the changes of $NaCl_{(aq)}$ droplet surface area and its temperature with processing time. The calculated data are in very good agreement with the experimental observations.

5. MODEL SIMULATION

The effects of processing parameters (i.e., gas temperature, solution concentration, and humidity) on the changes of an evaporating solution droplet were studied, using the mathematical model developed in the present work. The changes of droplet radius, droplet temperature, concentration field inside the droplet, and solvent evaporation rate were investigated.

Figure 5 gives the changes in radius, surface solute concentration, droplet temperature, and solvent evaporation rate for a solution droplet under the conditions described in Table 5. During evaporation, the surface concentration of solute increases rapidly while the droplet reduces its dimensions (Fig. 5(a)). When the surface concentration reaches the saturation values at the corresponding droplet temperatures, the solute starts to precipitate and the surface concentration will maintain its corresponding saturation values. Rapid increases of droplet temperatures are observed at the very beginning of evaporation and at the moment when solute precipitation started (the solid line in Fig. 5(b)). The dashed line in Fig. 5(b) shows the solvent evaporation rate. The evaporation rate increases very fast at the beginning and after

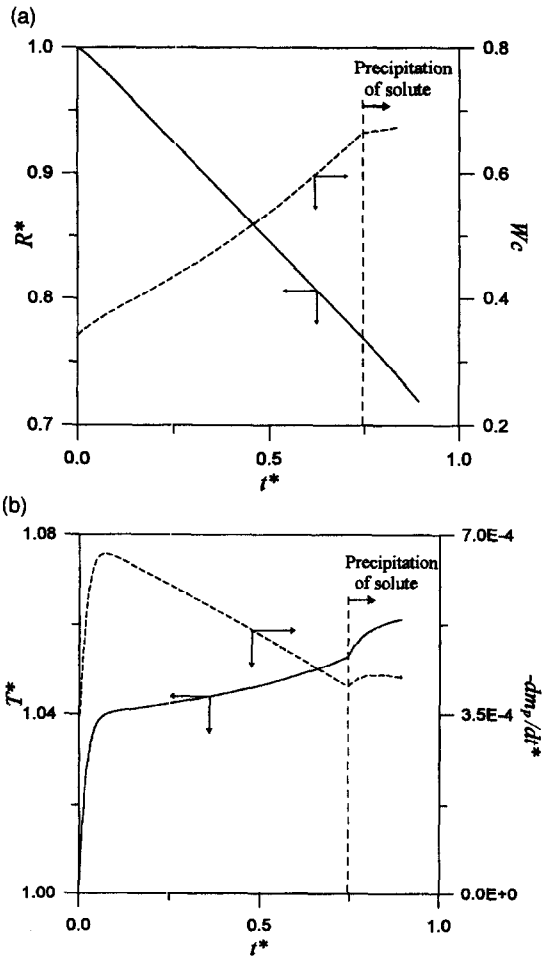

Fig. 5. Changes in (a) radius and surface solute concentration, and (b) temperature and solvent evaporation rate of $NH_4NO_{3(aq)}$ droplet.

Table 5. $NH_4NO_{3(aq)}$ droplet operating conditions

Temperature of air	323 K
Humidity of air	0%
System pressure	738 mmHg
Initial radius of droplet	0.0563 cm
Initial temperature of droplet	281 K
Initial mass fraction of solute	34%

reaching a maximum point, this rate decreases. When the droplet temperature jumps up due to the heat of precipitation, the solvent evaporation rate increases again. The solvent evaporation rate is governed by the variations of T^l, R, x_B, P^{sat}, and γ_B; the relationship among them can be expressed as [21]

$$-\frac{dm_P}{dt} \propto \frac{R\gamma_B x_B P^{sat}}{(T^l)^{0.125}}. \quad (9)$$

Initially P^{sat} rises rapidly with increasing droplet temperature and accordingly increases the rate of solvent evaporation. When the change of droplet temperature slows down, the variation of P^{sat} becomes insignificant. The evaporation rate is then governed by the products of R and x_B in eqn (9). When the droplet temperature jumps up again, P^{sat} rises and the rate of evaporation increases too.

Figure 6 shows the variations of solute concentrations inside the droplet at different processing times. When the solution droplet is just formed, the dissolved solute is uniformly distributed inside the droplet (curve 1 in Fig. 6). During evaporation, the size of the droplet decreases and a concentration gradient is developed inside the droplet (curves 2–6 in Fig. 6). Before precipitating the solute, the solute concentration on the droplet surface increases much faster than those far away from the surface. The surface concentration increases rapidly at the beginning of evaporation while the solute concentration at the center of the droplet rises slowly. When the surface concentration reaches the saturation value at the corresponding droplet temperature, the concentration gradient tends to decrease (curves 5 and 6 in Fig. 6).

The effects of gas temperature were studied, using three different gas temperatures: 298, 323 and 373 K. It is found that the increase of surrounding gas temperature raises the droplet temperature and accelerates the solvent evaporation, resulting in the increase of reduction rate of the droplet size and raising the rate of the surface solute concentration. Figure 7 shows the concentration gradients of solutes inside the droplet at the moment of crust formation. The concentration gradients for the droplet operated at higher gas temperatures are much steeper than those operated at lower gas temperatures. Less time is permitted for the solute to move inward to the center of the droplet when the solvent evaporation rate is higher.

Two different starting concentrations (i.e., $W_{CO} = 0.34$ and 0.5) were chosen to study the effects of initial solute concentration on the characteristics of evaporating droplets. Since a less concentrated aqueous solution provides a higher water vapor pressure

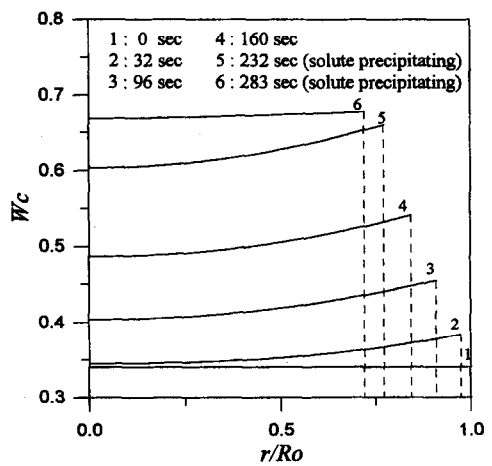

Fig. 6. Variation of concentration of ammonium nitrate inside the droplet at different times during evaporation.

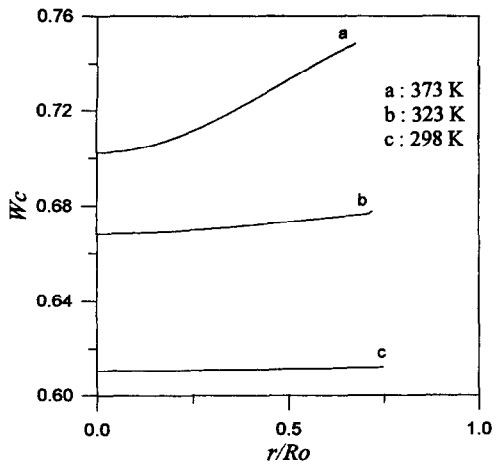

Fig. 7. Concentration gradients inside the $NH_4NO_{3(aq)}$ droplet at three different gas temperatures.

over the droplet surface and develops a bigger vapor concentration gap between the droplet surface and the bulk gas, a higher solvent evaporation rate is obtained for the starting solution at $W_{CO} = 0.34$. The high evaporation rate is responsible for the fast reduction of droplet size and the rapid increase of surface solute concentration; however, a longer time is required for those droplets of low concentrations to form the solid crust and smaller particles are then produced.

The study of the effects of humidity of the ambient gas indicates that although the increase of humidity slows down the solvent evaporation and raises the droplet temperature, the gas humidity does not have a significant impact on the concentration gradient of the droplet.

6. CONCLUSION

A mathematical model to describe the changes of an evaporating droplet was developed. In addition to the simultaneous consideration of the transfer of mass, momentum, and heat inside and around the droplet, the effects of solute precipitation were considered in the model. The concept of a real solution was employed in calculations to estimate the vapor pressure of solvent just above the surface of the droplet. This mathematical model was verified, using the available experimental data. The simulated results indicated that the movement of species inside the droplet was through both diffusion and convection. The evolved heat due to the precipitation of solutes caused the droplet temperature to jump up and accelerated the solvent evaporation. Increasing the gas temperature increased the solvent evaporation rate and caused a steeper concentration gradient to be built up inside the droplet. Decreasing the concentration of starting solution reduced the size of resultant particles. On the other hand, the effects of humidity of the ambient gas were found to be insignificant.

To avoid the formation of hollow particles in spray pyrolysis or spray drying, the concentration gradient inside the aerosol droplet needs to be minimized. Accordingly, a low processing temperature during evaporation and a dilute initial solution are desired to produce solid aerosol-derived particles. In other words, a two-stage heating arrangement in spray pyrolysis, which allows the solvent evaporation at lower temperatures followed by higher processing temperatures to complete required solid-state reactions, is suggested to produce solid aerosol-derived particles.

Acknowledgement—The authors are grateful to the National Science Council for partial support of this research under Grant No. NSC 84-2214-E-032-004.

REFERENCES

1. Gardner, T. J. and Messing, G. L., Preparation of MgO powder by evaporative decomposition of solutions. *Am. Ceram. Soc. Bull.*, 1984, **63**, 1498–1504.
2. Sproson, D. W., Messing, G. L. and Gardner, T. J., Powder synthesis for electronic ceramics by evaporative decomposition of solutions. *Ceram. Int.*, 1986, **12**, 3–7.
3. Gardalla, A. M. and Yu, H., Thermal decomposition of Fe(III) nitrate and its aerosol. *J. Mater. Res.*, 1990, **5**, 1233–1236.
4. Gadalla, A. M. and Yu, H., Preparation of fine, hollow, spherical $NiFe_2O_4$ powders. *J. Mater. Res.*, 1990, **5**, 2923–2927.
5. Gadalla, A. M. and Yu, H., Thermal behavior of Ni(II) nitrate hydrate and its aerosols. *J. Thermal Analysis*, 1991, **37**, 319–331.
6. Messing, G. L., Gardner, T. J. and Ciminelli, R. R., Characteristics of EDS-derived powders. *Science of Ceramics*, Vol. 12, pp. 117–124. Saint-Vincent, Italy, 1983.
7. Kodas, T. T., Engler, E. M., Lee, V. Y., Jacowitz, R., Baum, T. H., Roche, K. and Parkin, S. S. P., Aerosol flow reactor production of fine $Y_1Ba_2Cu_3O_7$ powder: fabrication of superconducting ceramics. *Appl. Phys. Lett.*, 1988, **52**, 1622–1624.
8. Ranz, W. E. and Marshall, W. R. Jr., Evaporation from drops: Part I and Part II. *Chem. Engr. Progress*, 1952, **48**, 141–146, 173–180.
9. Charlesworth, D. H. and Marshall, W. R., Jr. Evaporation from drops containing dissolved solids. *AIChE. J.*, 1960, **6**, 9–23.
10. El Golli, S., Bricard, J., Turpin, P.-Y. and Treiner, C., The evaporation of saline droplets, *J. Aerosol Sci.*, 1974, **5**, 273–292.
11. Leong, K. H., Morphology of aerosol particles generated from the evaporation of solution drops. *J. Aerosol Sci.*, 1981, **12**, 417–435.
12. Messing, G. L., Zhang, S. C. and Jayanthi, G. V., Ceramic powder synthesis by spray pyrolysis. *J. Am. Chem. Soc.*, 1993, **76**, 2707–2726.
13. Jayanthi, G. V., Zhang, S. C. and Messing, G. L., Modeling of solid particle formation during solution aerosol thermolysis. *Aerosol Sci. Technol.*, 1993, **19**, 478–490.
14. Yu, H., Modeling the changes in aerosol droplets of pure liquids and solutions due to evaporation, *Tamkang J.*, 1995, **34**, 157–183.
15. Yu, H., Simulation of spray pyrolysis for ceramic powder preparation. *Particulate Sci. Technol.*, 1995, **13**, 149–167.
16. Villadsen, J. and Micheisen, M. L., *Solution of Dif-*

ferential Equation Models by Polynomerial Approximation. Prentice, New York, 1978.
17. von Rosenberg, D. U., *Methods for the Numerical Solution of Partial Differential Equations*. Elsevier, New York, 1969.
18. Boynten, W. P. and Brattain, W. H., *International Critical Tables* (National Research Council, ed.). McGraw-Hill, New York, 1930, p. 62.
19. Reid, R. C., Prausnitz, J. M. and Sherwood, T. K., *The Properties of Gases and Liquids* (3rd edn). McGraw-Hill, New York, 1977.
20. Broul, M., Nijvlt, J. and Sihnel, O., In *Inorganic Two-component System*, Elsevier, New York, 1981.
21. Liao, W., Evaporation of solution droplets in spray pyrolysis, Master Thesis, Tamkang University, Tamsui, Taiwan (1996).